

An output feedback nonlinear decentralized controller for unmanned vehicle co-ordination

O. A. A. Orqueda^{*†}, X. T. Zhang and R. Fierro

Marhes Laboratory, School of Electrical and Computer Engineering, Oklahoma State University, Stillwater, OK 74078-5032, U.S.A.

SUMMARY

This paper presents vision-based control strategies for decentralized stabilization of *unmanned vehicle* formations. Three leader–follower formation control algorithms, which ensure asymptotic co-ordinated motion, are described and compared. The first algorithm is a *full state feedback* nonlinear controller that requires full knowledge of the leader's velocities and accelerations. The second algorithm is a *robust state feedback* nonlinear controller that requires knowledge of the rate of change of the relative position error. Finally, the third algorithm is an *output feedback* approach that uses a *high-gain observer* to estimate the derivative of the unmanned vehicles' relative position. Thus, this algorithm only requires knowledge of the leader–follower relative distance and bearing angle. Both data are computed using measurements from a single camera, eliminating sensitivity to information flow between vehicles. Lyapunov's stability theory-based analysis and numerical simulations in a realistic 3D environment show the stability properties of the control methodologies. Copyright © 2007 John Wiley & Sons, Ltd.

Received 7 October 2005; Revised 4 August 2006; Accepted 15 November 2006

KEY WORDS: formation stability; decentralized control; high-gain observers; sliding mode; artificial vision

1. INTRODUCTION

The problem of controlling groups of unmanned vehicles has gained interest in the recent years motivated by several exciting applications, such as automated transportation, spacecraft interferometry, mitigation of natural and man-made disasters, surveillance, mapping, border

*Correspondence to: O. A. A. Orqueda, School of Electrical and Computer Engineering, Oklahoma State University, 202 Engineering South, Stillwater, OK 74078-5032, U.S.A.

†E-mail: orqueda@ieee.org

Contract/grant sponsor: NSF; contract/grant number: #0311460

Contract/grant sponsor: CAREER; contract/grant number: #0348637

Contract/grant sponsor: U.S. Army Research Office; contract/grant number: DAAD19-03-1-0142

patrol, and search and rescue. In these applications, a system consisting of multiple cooperative robots is desirable because of its size, cost, flexibility, and fault tolerance [1].

Research on multi-vehicle system co-ordination has been focused both on *centralized* and *decentralized* control strategies. Centralized control strategies have the advantage of being able to reach a global optimum solution for tasks such as path planning and reconfiguration [2–4]. However, centralized algorithms become infeasible when the number of vehicles and constraints increase, preventing their implementation in real time. On the other hand, decentralized control approaches only require local information and can effectively achieve multi-vehicle co-ordination behaviours as the ones observed in flocks of birds or schools of fish. In these behaviours, individuals do not use explicit communication but local sensing in order to maintain a coherent formation or a co-ordinated motion, even when they have to move around obstacles or avoid predators [5–9].

Many approaches for solving multi-robot co-ordination problems reduce to a single-agent control problem by assuming that global communication of some co-ordination information is available. However, a co-ordination mechanism that does not rely on global communication ensures flexibility and mission safety because reference trajectories and mission objectives should not be shared among all agents but with some leaders [10]. Of course, this poses the challenge of designing robust and computationally simple formation controllers that can perform well in the presence of uncertainty in leaders' current and future states.

In the last few years, several motion co-ordination algorithms have been developed in the literature. In [11], the authors develop a formation control algorithm based on omnidirectional visual servoing and motion segmentation. Vision-based formation controllers are described in [12]. The algorithms use input–output linearization and require the estimation of leader–follower relative angle and leader's linear and angular velocities. Chen *et al.* [10] develop a decentralized control architecture that employs local sensor information. The information needed to implement the controller is the relative position and velocity between a robot and its leader. Another vision-based formation controller has been recently developed by Moshtagh *et al.* [9]. This distributed co-ordination approach is based on nearest-neighbour interactions, assuming that robots move with constant linear speed and achieve flocking after a given time. In general, flocking algorithms do not maintain a strict formation shape. Such formation maintenance is critical in applications such as cooperative payload transport [13], cooperative object pushing [14], and distributed sensor deployment when robots are to move forming certain geometric pattern [15].

In this paper, we present three leader–follower formation control algorithms. The first two are state feedback-based controllers that require total or partial knowledge of the state variables. On the other hand, the third algorithm, and main contribution of this paper, is a robust output feedback decentralized controller based only on monocular vision information about the relative motion between a robot and its designated leader. A high-gain observer (HGO) is used to estimate the derivatives of leader to follower distance and bearing angle. Moreover, this algorithm eliminates the need of inter-vehicle communication, increasing the reliability of the overall system.

The rest of the paper is organized as follows. In Section 2, we review some definitions on graph theory, robot formations, and briefly describe our vision system. The problem statement is given in Section 3. Section 4 describes and analyses the three nonlinear formation control algorithms developed in this paper. Section 5 provides several numerical simulation results in

a realistic 3D environment. Finally, we present our concluding remarks and future work in Section 6.

2. DEFINITIONS AND PRELIMINARY REMARKS

In this section, some of the basic concepts on graph theory and definitions relevant to multi-robot formations are summarized. The reader is referred to the references for a more detailed treatment [16–18].

2.1. Graph theory

A *directed graph* \mathcal{G} is a pair $(\mathcal{V}, \mathcal{E})$ of the set of vertices $\mathcal{V} \in \{1, \dots, N\}$ and directed edges $\mathcal{E} \in \mathcal{V} \times \mathcal{V}$, where an edge $(i, j) \in \mathcal{E}$ is an ordered pair of distinct vertices in \mathcal{V} , that it is said to be incoming with respect to the *head* j and outgoing with respect to the *tail* i . The *in degree* of a vertex is defined as the number of edges that have this vertex as head. If $i, j \in \mathcal{V}$ and $(i, j) \in \mathcal{E}$, then i and j are said to be *adjacent*, or *neighbours*, and are denoted by $i \sim j$. The *adjacency matrix* $A(\mathcal{G}) = \{a_{ij}\}$ of a graph \mathcal{G} is a matrix with non-zero elements such that $a_{ij} \neq 0 \Leftrightarrow i \sim j$. The set of *neighbours* of node i is defined by

$$\mathcal{N}_i := \{j \in \mathcal{V} \setminus \{i\} | a_{ij} \neq 0\}$$

A *weak path* of length r_p from vertex $i \in \mathcal{V}$ to vertex $j \in \mathcal{V}$ is a sequence of $r_p + 1$ distinct vertices, $v_1 = i, \dots, v_m, \dots, v_{r_p+1} = j$, such that for all $m \in [1, r_p]$, $(v_m, v_{m+1}) \in \mathcal{E}$ or $(v_{m+1}, v_m) \in \mathcal{E}$. A directed graph \mathcal{G} is *weakly connected* or simply *connected* if any two vertices can be joined with a weak path.

2.2. Mathematical model

Let us consider a multi-robot system composed of N_a agents modelled as unicycle-type velocity-controlled vehicles[‡] moving on the plane, with the kinematic model of the i th robot given by

$$\dot{q}_i(t) = \begin{bmatrix} \cos \theta_i(t) & 0 \\ \sin \theta_i(t) & 0 \\ 0 & 1 \end{bmatrix} u_i(t) \quad (1)$$

where $q_i(t) := [x_i(t), y_i(t), \theta_i(t)]^T \in SE(2)$ is the configuration vector with respect to an inertial reference frame, $(x_i, y_i) \in \mathbb{R}^2$ denotes the position in Cartesian co-ordinates, $\theta_i \in \mathcal{S} = (-\pi, \pi]$ is the heading angle, $u_i(t) := [v_i(t), \omega_i(t)]^T \in \mathcal{U}_i \subseteq \mathbb{R}^2$, $v_i(t)$, $\omega_i(t)$ are the linear and the angular velocities, respectively. Each agent is equipped with a vision sensor and a pan controller.

Let $\ell_{ij}(t) \in \mathbb{R}_{\geq 0}$, the relative Euclidean distance between robots i and j , be defined as

$$\ell_{ij}(t) := \sqrt{(x_i(t) - x_j(t))^2 + (y_i(t) - y_j(t))^2} \quad (2)$$

and let $\psi_{ij}(t) \in (-\pi, \pi]$, the relative bearing, be defined as

$$\psi_{ij}(t) := \pi + \zeta_{ij}(t) - \theta_i(t) \quad (3)$$

[‡]Note that other mathematical models can be adapted to this framework.

with $\zeta_{ij}(t) = a \tan 2(y_i(t) - y_j(t), x_i(t) - x_j(t))$. Let $\gamma_{ij}(t)$ be defined as

$$\gamma_{ij}(t) := \pi + \zeta_{ij}(t) - \theta_j(t) \tag{4}$$

as shown in Figure 1.

2.3. Vision system

In this subsection we briefly describe the vision system used in this work. We assume that each robot is equipped with a pan-controlled monochromatic camera and a truncated regular octagon shape with five identification tags, as shown in Figure 1.

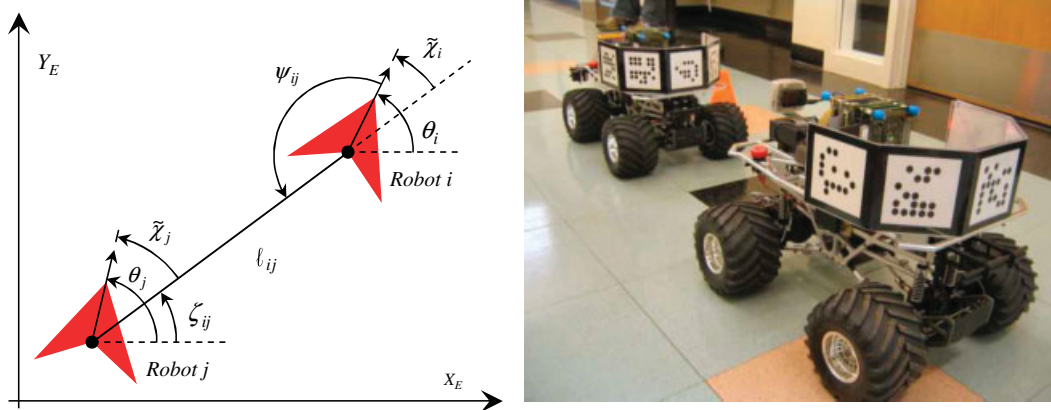


Figure 1. Relative distance and bearing.

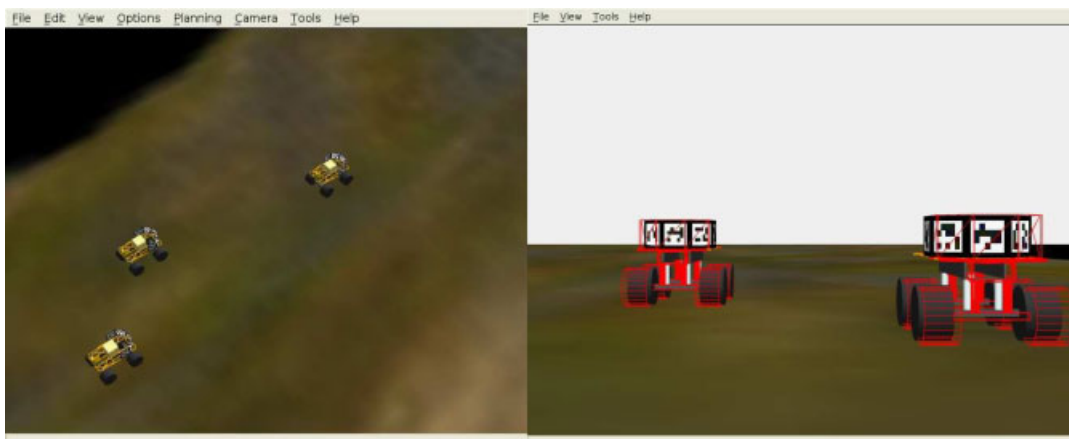


Figure 2. Estimated distances and bearings.

The position estimation algorithm can be divided into *identification* and *estimation*. Identification consists in determining an ID number for each robot, given by a code in every face of the octagon shape. Estimation consists in determining relative distance and orientation using the previously computed IDs, an off-line built database, and the POSIT algorithm [19].

Therefore, the vision system can obtain $\ell_{ij}(t)$, $\tilde{\chi}_i(t)$, and $\tilde{\chi}_j(t)$ from a single image, then $\psi_{ij}(t) = \pi - \tilde{\chi}_i(t)$ and $\gamma_{ij}(t) = \pi - \tilde{\chi}_j(t)$. Figure 2 shows an example of pose estimation in a virtual environment using this approach.

2.4. Formations

In this subsection, we define formations and formation control graphs. These definitions have been adapted from [17].

Definition 2.1 (Formation)

A *formation* is a network of vehicles interconnected *via* their controller specifications that dictate the distance and bearing each agent must maintain with respect to its leader. The interconnections between agents are modelled as edges in an acyclic directed graph, labelled by a given control specification.

Definition 2.2 (Formation control graph)

A formation control graph $\mathcal{G} = (\mathcal{V}, \mathcal{E}, \mathcal{S})$ is a directed acyclic graph consisting of:

- A finite set $\mathcal{V} = (v_1, \dots, v_{N_a})$ of N vertices and a map assigning to each vertex v_i a control system (1).
- An edge set $\mathcal{E} \subset \mathcal{V} \times \mathcal{V}$ encoding leader–follower relationships between agents. The ordered pair $(v_i, v_j) := e_{ij}$ belongs to \mathcal{E} when u_j depends on the state of agent i , q_i .
- A collection $\mathcal{S} = \{s_{ij}\}$ of edge specifications defines control objectives, or *set points*, for each agent $j : (v_i, v_j) \in \mathcal{E}$ for some $v_i \in \mathcal{V}$.

Leader agents regulate their behaviour to achieve group objectives, such as navigating in dynamic environments, or tracking reference paths.

3. PROBLEM STATEMENT

The co-ordination algorithms presented in this paper are based on the relative distance and bearing between a robot j and its *leader* i . Let $s_{ij}(t) \in \mathbb{R}^2$, the edge specification between robots i and j , be given by

$$s_{ij}(t) = [\ell_{ij}(t), \psi_{ij}(t)]^T \quad (5)$$

Taking time derivative of (5), we have

$$\dot{s}_{ij}(t) = -\varphi_1(z_{ij})v_j(t) - \varphi_2(z_{ij})v_i(t) - \varphi_3(z_{ij})\omega_i(t) \quad (6)$$

where $z_{ij} := [\ell_{ij}, \psi_{ij}, \gamma_{ij}]^T$ is a vector of known variables, and the vector fields $\varphi_1(z_{ij}), \varphi_2(z_{ij}), \varphi_3(z_{ij}) \in \mathbb{R}^2$ are given by

$$\varphi_1(z_{ij}) := \begin{bmatrix} -\cos \gamma_{ij} \\ \frac{\sin \gamma_{ij}}{\ell_{ij}} \end{bmatrix}, \quad \varphi_2(z_{ij}) := \begin{bmatrix} \cos \psi_{ij} \\ -\frac{\sin \psi_{ij}}{\ell_{ij}} \end{bmatrix}, \quad \varphi_3(z_{ij}) := \begin{bmatrix} 0 \\ 1 \end{bmatrix} \tag{7}$$

Taking time derivative of (6), it yields

$$\ddot{s}_{ij}(t) = -g(z_{ij}, v_j)\omega_j(t) - g_0(z_{ij}, v_j) - g_s(z_{ij}, v_j)\dot{s}_{ij}(t) - g_v(z_{ij}, v_j)V_i(t) \tag{8}$$

with

$$g(z_{ij}, v_j) := \begin{bmatrix} -\cos \gamma_{ij} & -v_j \sin \gamma_{ij} \\ \frac{\sin \gamma_{ij}}{\ell_{ij}} & -\frac{v_j \cos \gamma_{ij}}{\ell_{ij}} \end{bmatrix} \in \mathbb{R}^{2 \times 2} \tag{9}$$

$$g_0(z_{ij}, v_j) := \begin{bmatrix} -\frac{v_j^2(t)}{\ell_{ij}} \\ 0 \end{bmatrix} \in \mathbb{R}^{2 \times 2} \tag{10}$$

$$g_s(z_{ij}, v_j) := \begin{bmatrix} \frac{v_j \cos \gamma_{ij}}{\ell_{ij}} & 0 \\ -\frac{2v_j \sin \gamma_{ij}}{\ell_{ij}^2} & 0 \end{bmatrix} \in \mathbb{R}^{2 \times 2} \tag{11}$$

$$g_v(z_{ij}, v_j) := \begin{bmatrix} v_j \frac{2 \cos \theta_{ij} - \cos \gamma_{ij} \cos \psi_{ij}}{\ell_{ij}} & \cos \psi_{ij} & -\frac{\sin^2 \psi_{ij}}{\ell_{ij}} & 0 & \sin \psi_{ij} \\ \frac{2v_j \cos \gamma_{ij} \sin \psi_{ij}}{\ell_{ij}^2} & -\frac{\sin \psi_{ij}}{\ell_{ij}} & -\frac{\sin 2\psi_{ij}}{\ell_{ij}^2} & 1 & \frac{\cos \psi_{ij}}{\ell_{ij}} \end{bmatrix} \in \mathbb{R}^{2 \times 5} \tag{12}$$

The basic control vector is defined by

$$\omega_j(t) := \begin{bmatrix} \dot{v}_j(t) \\ \omega_j(t) \end{bmatrix} \in \mathbb{R}^2 \tag{13}$$

and the control vector of leader’s velocities and accelerations is defined as

$$V_i(t) := [v_i(t), \dot{v}_i(t), v_i^2(t), \dot{\omega}_i(t), v_i(t)\omega_i(t)]^T \in \mathbb{R}^5$$

Remark 3.1

Usually $V_i(t)$ is unknown.

It is easy to verify that the input matrix transformation $g(z_{ij}, v_j)$ in (9) is non-singular if $v_j(t) \geq v_{\min} > 0$ and $\ell_{ij}(t) \geq \ell_{\min} > 0$, where v_{\min} is the minimum speed of the follower robot, and ℓ_{\min} is the minimum distance required between robots to avoid collision.

The objective is to design a control law $u_j(t)$, based on (13), that allows robot j to track its leader i with a desired relative distance and bearing, $s_{ij}^d(t) \in \mathbb{R}^2$. Then, let the *tracking error* be defined as

$$e(t) := s_{ij}^d(t) - s_{ij}(t), \quad e(t) \in \mathbb{R}^2 \tag{14}$$

Taking first- and second-time derivatives of (14), and using (6), (8), it follows:

$$\dot{e}(t) = \dot{s}_{ij}^d(t) + \varphi_1(z_{ij})v_j(t) + \varphi_2(z_{ij})v_i(t) + \varphi_3(z_{ij})\omega_i(t) \tag{15}$$

$$\ddot{e}(t) = g(z_{ij}, v_j)\omega_j(t) + \phi(\dot{s}_{ij}, z_{ij}, v_j) + g_v(z_{ij}, v_j)V_i(t) \tag{16}$$

with

$$\phi(\dot{s}_{ij}, z_{ij}, v_j) := \ddot{s}_{ij}^d(t) + g_0(z_{ij}, v_j) + g_s(z_{ij}, v_j)\dot{s}_{ij}(t) \tag{17}$$

Let the filtered error signal $r(t) = [r_1(t), r_2(t)]^T \in \mathbb{R}^2$ be defined as

$$r(t) := \dot{e}(t) + Ke(t) \tag{18}$$

where $K = \text{diag}(k_1, k_2)$, $k_1, k_2 \in \mathbb{R}_{>0}$ are positive gain constants. Differentiating (18) with respect to time and using (16) yields

$$\dot{r}(t) = g(z_{ij}, v_j)\omega_j(t) + \phi(\dot{s}_{ij}, z_{ij}, v_j) + g_v(z_{ij}, v_j)V_i(t) + K\dot{e}(t) \tag{19}$$

4. FORMATION CONTROL ALGORITHMS

In this section, three state feedback controllers are described. The first one assumes full knowledge of the states of leader i in (16). The second approach assumes knowledge of the derivative of the specification $\dot{s}_{ij}(t)$. Both controllers are motivated by ideas from the well-established area of input–output feedback linearization [20]. The third controller is an output feedback controller which only needs knowledge of the edge specification $s_{ij}(t)$, i.e. the relative distance and bearing. The three controllers use the following assumption.

Assumption 1

Leader robot i is stably tracking some well-behaved desired trajectory $u_i^d(t) := [v_i^d(t), \omega_i^d(t)]^T \in \mathbb{R}^2$, with $u_i^d(t), \dot{u}_i^d(t), \ddot{u}_i^d(t) \in \mathcal{L}_\infty$. Consequently, it is assumed that $u_i(t), \dot{u}_i(t), \ddot{u}_i(t) \in \mathcal{L}_\infty$.

4.1. Full state feedback formation control (FSFB)

The first control law is equivalent to the one originally presented in [21] for first-order dynamics. It assumes full knowledge of all states of robot j and its leader i in (16). The control input is given by

$$\varpi_j(t) = -g^{-1}(z_{ij}, v_j)[\phi(\dot{s}_{ij}, z_{ij}, v_j) + g_v(z_{ij}, v_j)V_i(t) + 2K\dot{e}(t) + K^2e(t)] \quad (20)$$

with K defined in (18). Replacing (20) into (16), the error dynamics of the closed-loop system become

$$\ddot{e}(t) + 2K\dot{e}(t) + K^2e(t) = 0 \quad (21)$$

Therefore, because the characteristic equation (21) is Hurwitz and critically damped, the error $e(t)$ tends exponentially to zero as $t \rightarrow \infty$.

It is important to note that the FSFB controller (20) can achieve the control objective only when leader's velocities are available.

4.2. Robust state feedback formation control (RSFB)

This controller uses Assumption 1 and the following assumption.

Assumption 2

Leader's velocity and acceleration, $u_i(t)$ and $\dot{u}_i(t)$, are unknown. However, the derivative of edge specification $\dot{s}_{ij}(t)$ in (6) is perfectly known by measurement or estimation.

Then, let the RSFB control law $\varpi_j(t)$ be designed as

$$\varpi_j(t) = -g^{-1}(z_{ij}, v_j)[\phi(\dot{s}_{ij}, z_{ij}, v_j) + 2K\dot{e}(t) + K^2e(t) + \bar{u}_j(t)] \quad (22)$$

where $\bar{u}_j(t) \in \mathbb{R}^2$ is an auxiliary control law defined as

$$\bar{u}_j(t) := \beta \text{sign}(e(t)) \quad (23)$$

with $\beta \in \mathbb{R}_{>0}$ a positive control gain. As usual, the function $\text{sign}(\cdot)$ is defined as

$$\text{sign}(x) := \begin{cases} 1 & \text{if } x > 0 \\ 0 & \text{if } x = 0 \\ -1 & \text{if } x < 0 \end{cases}$$

The closed-loop system is obtained by substituting (22) into (19), thus

$$\dot{r}(t) = -Kr(t) + g_v(z_{ij}, v_j)V_i(t) - \bar{u}_j(t) \quad (24)$$

Before presenting the stability proof of the closed-loop system (24), it is necessary to state the following lemma.

Lemma 4.1

Let the auxiliary function $L(t) \in \mathbb{R}$ be defined as

$$L(t) := r^T(t)[g_v(z_{ij}, v_j)V_i(t) - \bar{u}_j(t)] \quad (25)$$

If the control gain β is selected to satisfy the sufficient condition

$$\beta > \|g_v(z_{ij}, v_j)V_i(t)\|_2 + k_{12}^{-1} \left\| \frac{d[g_v(z_{ij}, v_j)V_i(t)]}{dt} \right\|_2$$

where K is given in (18) and $k_{12} := \min(k_1, k_2)$. Then

$$\int_{t_0}^t L(\tau) d\tau < \zeta_b$$

where the positive constant $\zeta_b \in \mathbb{R}_{>0}$ is defined as

$$\zeta_b := \beta \|e(t_0)\|_1 - e^T(t_0)[g_v(z_{ij}(t_0), v_j(t_0))V_i(t_0)] \tag{26}$$

and $\|\cdot\|_1$ denotes the \mathcal{L}_1 norm.

Proof

See Appendix. □

The following theorem states the stability of the closed-loop system (24).

Theorem 4.2

Control law (22) and auxiliary control law (23) ensure that the system is asymptotically stable, all its variables are bounded, and the tracking error and its derivative tend to zero, that is

$$e(t), \dot{e}(t) \rightarrow 0 \quad \text{as } t \rightarrow \infty \tag{27}$$

Proof

Let the function $P(t) \in \mathbb{R}$ be defined as

$$P(t) := \zeta_b - \int_{t_0}^t L(\tau) d\tau \geq 0 \tag{28}$$

where ζ_b and $L(t)$ are defined in (25) and (26), respectively. Based on the non-negativity of $P(t)$, let the Lyapunov function candidate $V(t)$ be defined as

$$V(t) := \frac{1}{2} r^T(t)r(t) + P(t) \tag{29}$$

Taking time derivative of (29), using (24), (25), and (28), it follows

$$\dot{V}(t) = -r^T(t)Kr(t) \leq -k_{12}\|r(t)\|^2 \tag{30}$$

with $k_{12} := \min(k_1, k_2)$. Therefore, $V(t) \in \mathcal{L}_\infty \cap \mathcal{L}_2$, then $r(t)$ and $P(t) \in \mathcal{L}_\infty \cap \mathcal{L}_2$. From (18), it is clear that $e(t), \dot{e}(t) \in \mathcal{L}_\infty$, and from (24), it can be seen that $\dot{r}(t) \in \mathcal{L}_\infty$; then $\dot{V}(t) \in \mathcal{L}_\infty$. Considering that $V(t)$ is lower bounded by $\|r(t)\|^2$, by the Barbalat's lemma $\lim_{t \rightarrow \infty} \dot{V}(t) = 0$. This means that $\lim_{t \rightarrow \infty} k_{12}\|r(t)\|^2 = 0$, or $r(t) \rightarrow 0$ as $t \rightarrow \infty$ by Rayleigh–Ritz theorem [22]. Since (18) is a stable first-order differential equation driven by $r(t)$, it can be ensured that $\lim_{t \rightarrow \infty} e(t) = 0$ and $\lim_{t \rightarrow \infty} \dot{e}(t) = 0$. □

4.3. Output feedback formation control algorithm (OFB)

In the previous subsection, a RSFB control law was designed that did not require the knowledge of the leader's speed and acceleration, but the knowledge of $s_{ij}(t)$, something difficult to obtain in practice. In this subsection, the RSFB controller is extended to an OFB control algorithm to avoid this drawback.

Let the unknown vector $\dot{s}_{ij}(t)$ be estimated using a HGO [23] as follows:

$$\dot{\hat{s}}_1(t) = \hat{s}_2(t) + \frac{\alpha_1}{\varepsilon} (s_{ij}(t) - \hat{s}_1(t)) \quad (31)$$

$$\dot{\hat{s}}_2(t) = -g(z_{ij}, v_j)\omega_j(t) - g_0(z_{ij}, v_j) - g_s(z_{ij}, v_j)\hat{s}_2 + \frac{\alpha_2}{\varepsilon^2} (s_{ij}(t) - \hat{s}_1(t)) \quad (32)$$

where $\alpha_1, \alpha_2 \in \mathbb{R}_{>0}^{2 \times 2}$ are constant diagonal matrices, called *HGO gains*, and $\varepsilon \in \mathbb{R}_{>0}$ is the HGO constant. The HGO gains are chosen such that the roots of

$$s^2 + \alpha_1 s + \alpha_2 = 0$$

have negative real parts. The HGO constant has to be designed such that the estimated variable, $\hat{s}_2(t)$, converges to the real values, $s_{ij}(t)$, fast enough to stabilize the whole system. Let the estimation errors be defined as

$$\eta_1(t) = \frac{1}{\varepsilon} (s_{ij}(t) - \hat{s}_1(t)) \quad (33)$$

$$\eta_2(t) = \dot{s}_{ij}(t) - \hat{s}_2(t) \quad (34)$$

Using (31)–(34), the dynamic observer error system is given by

$$\varepsilon \dot{\eta}_1(t) = -\alpha_1 \eta_1(t) + \eta_2(t) \quad (35)$$

$$\varepsilon \dot{\eta}_2(t) = -\alpha_2 \eta_2(t) - \varepsilon [g_s(z_{ij}, v_j)\eta_2 + g_v(z_{ij}, v_j)V_i(t)] \quad (36)$$

Let the vector $\eta(t)$ be defined as $\eta(t) := [\eta_1^T(t), \eta_2^T(t)]^T \in \mathbb{R}^4$, then

$$\varepsilon \dot{\eta}(t) = A_0 \eta(t) + \varepsilon f(t) \quad (37)$$

where

$$A_0 = \begin{bmatrix} -\alpha_1 & I_2 \\ -\alpha_2 & 0_2 \end{bmatrix} \in \mathbb{R}^{4 \times 4}, \quad 0_2 \in \mathbb{R}^{2 \times 2}$$

is a null matrix, $I_2 \in \mathbb{R}^{2 \times 2}$ is an identity matrix, and

$$f(t) = \begin{bmatrix} 0 \\ -g_s(z_{ij}, v_j)\eta_2 - g_v(z_{ij}, v_j)V_i(t) \end{bmatrix} \in \mathbb{R}^4$$

If $\varepsilon \rightarrow 0$ and $d\tau = (1/\varepsilon) dt$ in (37), then

$$\frac{d\eta(\tau)}{d\tau} = A_0\eta(\tau) \tag{38}$$

Equation (38) is called the *boundary layer system*.

Let $W(\eta)$ be a non-negative function for the boundary layer system defined as

$$W(\eta) = \eta^T P_0 \eta \tag{39}$$

where $P_0 \in \mathbb{R}^{4 \times 4}$ is a positive definite matrix such that $P_0 A_0 + A_0^T P_0 = -I_4$, then

$$\frac{dW}{d\tau} = \frac{d\eta^T}{d\tau} P_0 \eta + \eta^T P_0 \frac{d\eta}{d\tau} = -\|\eta\|^2 \leq 0 \tag{40}$$

Consequently, the boundary layer system has the properties

$$\begin{aligned} \lambda_{\min}(P_0)\|\eta\|^2 &\leq W(\eta) \leq \lambda_{\max}(P_0)\|\eta\|^2 \\ \dot{W} = \frac{\partial W}{\partial \eta} \dot{\eta} &\leq -\lambda_\omega \|\eta\|^2, \quad 0 \leq \lambda_\omega \leq 1 \\ \left\| \frac{\partial W}{\partial \eta} \right\| &\leq 2\|P_0\|\|\eta\|, \quad \|P_0\| = \lambda_{\max}(P_0) \end{aligned} \tag{41}$$

From (41), it is clear that the origin $\eta(t) = [0, 0, 0, 0]^T$ is a globally exponentially stable equilibrium of (38). The solution for the error dynamics (35)–(36), $\eta(t)$, contains terms of the form $(1/\varepsilon)e^{-\omega t/\varepsilon}$, for some $\omega > 0$. Note that $\eta(t)$ can be very large if ε is small enough, because its amplitude is $O(1/\varepsilon)$. Then, the new feedback control design based on HGO is saturated to avoid the peaking phenomenon on $\eta(t)$,

$$\varpi_j(t) = \text{sat} \{ -g^{-1}(z_{ij}, v_j) [\phi(\hat{s}_2, z_{ij}, v_j) + 2K(s_{ij}^d(t) - \hat{s}_2(t)) + K^2 e(t) + \bar{u}_j(t)] \} \tag{42}$$

Remark 4.3

The RSFB controller (22) designed in Section 4.3 is globally asymptotically stable. Theoretically, the observer error will not cause the system to become unstable using the OFB controller (42), but it is still necessary to use saturation to prevent over-exceeding the control strength due to peaking phenomenon.

The closed-loop formation tracking error dynamics under the OFB control law (42) is

$$\dot{r}(t) = -Kr(t) - 2K\eta_2(t) + g_s(z_{ij}, v_j)\eta_2(t) + g_v(z_{ij}, v_j)V_i(t) - \bar{u}_j(t) \tag{43}$$

4.3.1. Stability analysis of the OFB controller. In this subsection, we prove that the combined closed-loop system (37) and (43) is asymptotically stable. The proof is done in three steps: in the first step, it is shown that there exists an invariant set for the closed loop OFB system based on a composite Lyapunov function. In the second step, we show that any trajectory will be trapped into this invariant set in finite time if the HGO constant ε is chosen small enough. In the third step, it is demonstrated that this invariant set is globally uniformly ultimately bounded (GUUB).

Let $\mathcal{R} = \mathbb{R}^2$ be the region of attraction of system (16) with control law (42). Let \mathcal{D}_r be a compact set in the interior of \mathcal{R} . Let the compact set \mathcal{D}_c , which contains the origin of (43), be defined by $\mathcal{D}_c := \{r(t) \in \mathcal{R} | V(t) \leq c\}$, where $V(t)$ is defined in (29) and $c > \max_{r \in \partial \mathcal{D}_r} V(t)$ is a small positive constant. The set \mathcal{D}_c is a compact subset of \mathcal{R} and \mathcal{D}_r is in the interior of \mathcal{D}_c . Let the compact set \mathcal{D}_ε be defined by $\mathcal{D}_\varepsilon := \{\eta(t) \in \mathbb{R}^4 | W(t) \leq \rho \varepsilon^2\}$, where $W(t)$ is given in (39), ρ is a positive constant to be selected later, and ε is the HGO constant. Finally, let the set Σ_c be defined as $\Sigma_c := \mathcal{D}_c \times \mathcal{D}_\varepsilon \in \mathbb{R}^6$.

The derivative of (29) for $(e(t), \dot{e}(t), \eta(t)) \in \{V(t) = c\} \times \mathcal{D}_\varepsilon$ verifies

$$\begin{aligned} \dot{V}(t) &\leq -k_{12} \|r(t)\| [\|r(t)\| - \sigma_1 \|\eta(t)\|] \\ &\leq -k_{12} \mu (\mu - L_1 \varepsilon) \end{aligned} \tag{44}$$

with $\sigma_1 := (\sigma_s + 2\bar{k}_{12})/k_{12}$, $\sigma_s := \max_{z_{ij}} \|g_s(z_{ij}, v_j)\|$, $\bar{k}_{12} := \max(k_1, k_2)$, $\mu = \min_{r \in \partial \mathcal{D}_c} \{\|r(t)\|\}$, and $L_1 := \sigma_1 \sqrt{\rho/\lambda_{\min}(P_0)}$.

Analysing the derivative of (39) for $(e(t), \dot{e}(t), \eta(t)) \in \mathcal{D}_c \times \{W(t) = \rho \varepsilon^2\}$ we find

$$\begin{aligned} \dot{W}(t) &\leq -\frac{\|\eta(t)\|^2}{2\varepsilon} (1 - 4\|P_0\| \sigma_s \varepsilon) - \frac{\|\eta(t)\|}{2\varepsilon} [\|\eta(t)\| - 4\|P_0\| \sigma_v \varepsilon] \\ &\leq -\frac{\|\eta(t)\|^2}{2\varepsilon} (1 - 4\|P_0\| \sigma_s \varepsilon) - \frac{\|\eta(t)\|}{2} \left(\sqrt{\frac{\rho}{\|P_0\|}} - 4\|P_0\| \sigma_v \right) \end{aligned} \tag{45}$$

with $\sigma_v := \max_{z_{ij}, u_i} \|g_v(z_{ij}, v_j) V_k(t)\|$.

Taking $\rho = 16\sigma_v^2 \|P_0\|^3$ and $\varepsilon_1 = \min(1/4\sigma_s \|P_0\|, \mu/L_1)$, for every $0 < \varepsilon \leq \varepsilon_1$, we have

$$\dot{V}(t) \leq 0$$

for $(e(t), \dot{e}(t), \eta(t)) \in \{V(t) = c\} \times \mathcal{D}_\varepsilon$, and

$$\dot{W}(t) \leq 0$$

for $(e(t), \dot{e}(t), \eta(t)) \in \mathcal{D}_c \times \{W(t) = \rho \varepsilon^2\}$. Therefore, Σ_c is a positively invariant set.

Let us show that the trajectory of the system is trapped in this set. The initial state satisfy $(e(0), \dot{e}(0), \eta(0)) \in \mathcal{D}_r \times \mathcal{Q}$, where \mathcal{Q} is a compact set such that $\mathcal{Q} \subseteq \mathbb{R}^4$. Using (33)–(34) it can be seen that

$$\|\eta(0)\| \leq \frac{c_3}{\varepsilon}$$

where $c_3 \in \mathbb{R}_{>0}$ is an appropriate constant. Because $(e(0), \dot{e}(0)) \in \mathcal{D}_r$, we have

$$\begin{aligned} \|e(t) - e(0)\| &\leq c_2^a t \\ \|\dot{e}(t) - \dot{e}(0)\| &\leq c_2^b t \\ \|r(t) - r(0)\| &\leq c_2 t \end{aligned} \tag{46}$$

where $c_2^b, c_2^a, c_2 \in \mathbb{R}_{>0}$ are some positive constants. Therefore, there exists a finite time T_0 , independent of ε , such that $(e(t), \dot{e}(t)) \in \mathcal{D}_r$ for all $t \in [0, T_0]$. In consequence, when $t \in [0, T_0]$ and $W(\eta(t)) \geq \rho \varepsilon^2$, from (45), $\dot{W}(t) \leq -(1/2\varepsilon) \|\eta(t)\|^2$. Then

$$\dot{W}(t) \leq -\frac{\mu_1}{\varepsilon} W(t) \tag{47}$$

with $\mu_1 := 1/2\|P_0\|$. The solution for (47) is

$$W(t) \leq \frac{\mu_2}{\varepsilon^2} \exp\left(-\frac{\mu_1}{\varepsilon} t\right) \tag{48}$$

with $\mu_2 := c_3^2\|P_0\|$. As it can be seen from (48), $\lim_{t \rightarrow \infty} W(t) = 0$. Let T_ε be the time for which $W(t)$ falls below to $\rho\varepsilon^2$, it must satisfy

$$W(\eta(T_\varepsilon)) \leq \frac{\mu_2}{\varepsilon^2} \exp\left(-\frac{\mu_1}{\varepsilon} T_\varepsilon\right) \leq \rho\varepsilon^2 \tag{49}$$

In consequence, $T_\varepsilon \geq (\varepsilon/\mu_1) \ln(\mu_2/\rho\varepsilon^4)$ and $\lim_{\varepsilon \rightarrow 0} T_\varepsilon = 0$. Then, it is possible to choose ε_2 small enough such that $T_\varepsilon = \frac{1}{2}T_0$, for all $\varepsilon \in (0, \varepsilon_2]$. It follows that $W(\eta(T_\varepsilon)) < \rho\varepsilon^2$ for all $\varepsilon \in (0, \varepsilon_2]$. Choosing $\varepsilon_1^* = \min(\varepsilon_1, \varepsilon_2)$, the trajectory $(e(t), \dot{e}(t), \eta(t))$ enters into the invariant set Σ_c in $t \in [0, T_\varepsilon]$ and remains in Σ_c , for all $t \geq T_\varepsilon$ and every $0 < \varepsilon \leq \varepsilon_1^*$. Moreover, the trajectory $(e(t), \dot{e}(t), \eta(t))$ is bounded by (46) and (48), for $t \in [0, T_\varepsilon]$ and $\varepsilon \in (0, \varepsilon_1^*]$.

If the initial state satisfies $(e(0), \dot{e}(0), \eta(0)) \in \mathcal{D}_r \times \mathcal{Q}$, then the trajectory of the system will be inside Σ_c , for all $t \geq T_\varepsilon$ and $0 < \varepsilon \leq \varepsilon_1^*$. Because, from (48), $\lim_{\varepsilon \rightarrow 0} W(\eta(t)) = 0$, it is possible to find $\varepsilon_3 = \varepsilon_3(\delta_0) \leq \varepsilon_1^*$, for any given small value δ_0 , such that

$$\|\eta(t)\| \leq \frac{\delta_0}{2} \tag{50}$$

for $t \geq T_{\varepsilon_3} = T_{\varepsilon_3}(\delta_0)$.

Let the compact sets \mathcal{D}_1 and \mathcal{D}_2 be given by

$$\mathcal{D}_1 := \{(e(t), \dot{e}(t)) \in \mathcal{R} : \|r(t)\|^2 \leq 2L_1\varepsilon\} \tag{51}$$

and

$$\mathcal{D}_2 := \{(e(t), \dot{e}(t)) \in \mathcal{R} : V(t) \leq v(\varepsilon)\} \tag{52}$$

with $v(\varepsilon) := \max_{\|r\|^2 < 2L_1\varepsilon} \{V(t)\}$. If $(e(t), \dot{e}(t)) \notin \mathcal{D}_1$,

$$\dot{V}(t) \leq -\frac{1}{2}k_{12}\|r(t)\|^2$$

Let $\varepsilon_4 = \varepsilon_4(\delta_0)$ be chosen such that \mathcal{D}_2 is in the interior of \mathcal{D}_c and

$$\mathcal{D}_2 \subset \{(e(t), \dot{e}(t)) \in \mathcal{R} : \|e(t)\| \leq \frac{1}{4}\delta_0, \|\dot{e}(t)\| \leq \frac{1}{4}\delta_0\}$$

Then for all $(e(t), \dot{e}(t)) \in \mathcal{D}_c$, $(e(t), \dot{e}(t)) \notin \mathcal{D}_2$

$$\dot{V}(t) \leq -\frac{1}{2}k_{12}\|r(t)\|^2$$

Therefore, the set $\Sigma_1 := \mathcal{D}_2 \times \mathcal{D}_\varepsilon$ is positively invariant and every trajectory in $\mathcal{D}_c \times \mathcal{D}_\varepsilon$ enters Σ_1 in finite time $T_{\varepsilon_4} = T_{\varepsilon_4}(\delta_0)$, for $\varepsilon \in (0, \varepsilon_4]$. Let $\varepsilon_2^* = \min\{\varepsilon_3, \varepsilon_4\}$ and $T_1 = \max\{T_{\varepsilon_3}, T_{\varepsilon_4}\}$, therefore

$$\|e(t)\| + \|\dot{e}(t)\| + \|\eta(t)\| \leq \delta_0 \tag{53}$$

with $\delta_0 > 0$, $\varepsilon \in (0, \varepsilon_2^*]$, and $t \geq T_1$. Then $(e(t), \dot{e}(t), \eta(t))$ is GUUB.

5. SIMULATION RESULTS

In this section, simulations are presented that validate the performance of the decentralized control algorithms designed herein. All simulations were written in C++ on a Linux platform using MPSLab,[§] a motion planning, simulation, and virtual perception software library written by one of the authors [24, 25].

The initial positions of the robots in simulations shown in Figures 3–13 are $q_\ell(0) = [0, 0, 0]^T$, $q_1^1(0) = [-2, -1, 0]^T$, and $q_2^2(0) = [-2, 1, 0]^T$, and their initial velocities are equal to 0.01. The parameters of the controllers are $k_1 = k_2 = \beta = 5.0$, the sampling time is 10 ms, the edge specifications are $s_{1\ell}^d = [2.0, -\frac{3}{4}\pi]^T$ and $s_{2\ell}^d = [2.0, \frac{3}{4}\pi]^T$. To avoid excessive chattering, the function is used

$$\bar{u}_j(t) := \beta \tanh(24.53 e(t))$$

In the first case, shown in Figures 3–7, the leader follows a straight line path with constant velocity $u_i(t) = [1.0 \text{ m/s}, 0.0 \text{ rad/s}]^T$. In the second case, depicted in Figures 8–12, the leader follows a circular path with constant velocity $u_i(t) = [1.0 \text{ m/s}, 0.3 \text{ rad/s}]^T$. The velocity bounds for the follower vehicles are $|v_j(t)| \leq 1.6$ and $|\omega_j(t)| \leq 11.5$, $j = 1, 2$.

The decentralized controller is able to drive each robot to the desired relative distance and desired bearing angle. Figures 3 and 8 show the trajectories of the robots by using the OFB controller with $\varepsilon = 0.001$. Figures 4 and 9, and Figures 5 and 10 show the decentralized control inputs and the tracking error of follower 1 for the three controllers, with linear and circular trajectories, respectively. It should be noted that not only the tracking error but also the control effort degrade. Notwithstanding, the behaviour using the OFB controller is quite satisfactory.

Figures 6 and 11, and Figures 7 and 12 illustrate the effects of the selection of the HGO constant ε on the control input and the tracking error, respectively. As ε decreases, tracking errors decrease and control efforts increase during the transient response, when the observer has not achieved steady state.

Figures 13 and 14 show simulations of the OFB controller with three- and seven-robot systems in the 3D simulation environment MPSLab. Figure 15 shows the edge specification for the simulation shown in Figure 14. As it can be seen, the results in the environment MPSLab are quite remarkable.

6. CONCLUSIONS

This paper presents a robust multi-vehicle output feedback (OFB) decentralized controller. Using the main result of this work, an OFB controller, each robot only requires a single camera to maintain a specified formation shape. The formation specification is given by the relative distance and bearing angle between each robot and its leader. A HGO is used to estimate the states of the robot and its neighbour(s).

A theoretical analysis based on Lyapunov stability theory has been performed to prove asymptotic stability of the RSFB formation controller (Section 4.2), and GUUB stability of the OFB formation controller (Section 4.3).

[§]<http://marhes.okstate.edu/~orqueda/mpslab.html>.

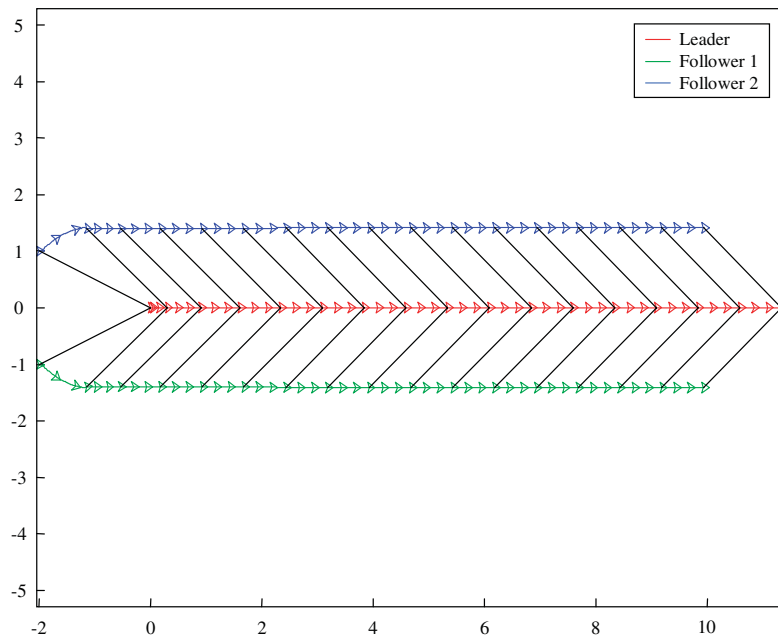


Figure 3. Trajectories of the leader robot and two followers for the straight line path case.

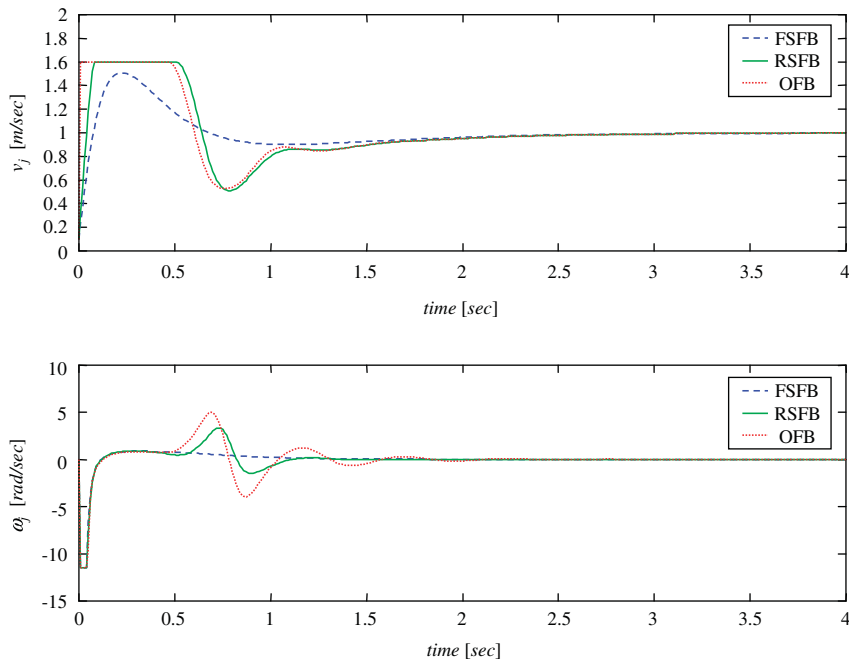


Figure 4. Velocity comparison between controllers (20), (22), and (42) for the straight line path case.

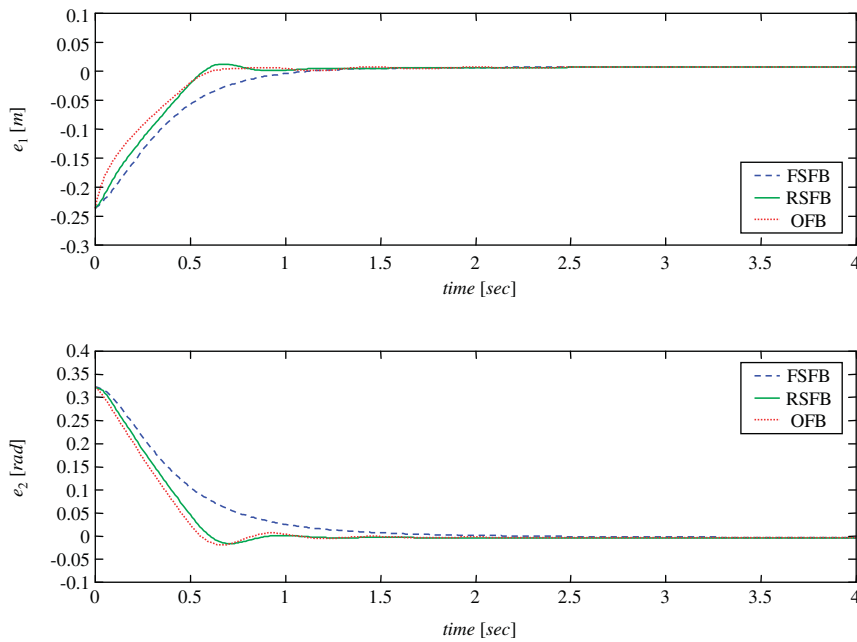


Figure 5. Error comparison between controllers (20), (22), and (42) for the straight line path case.

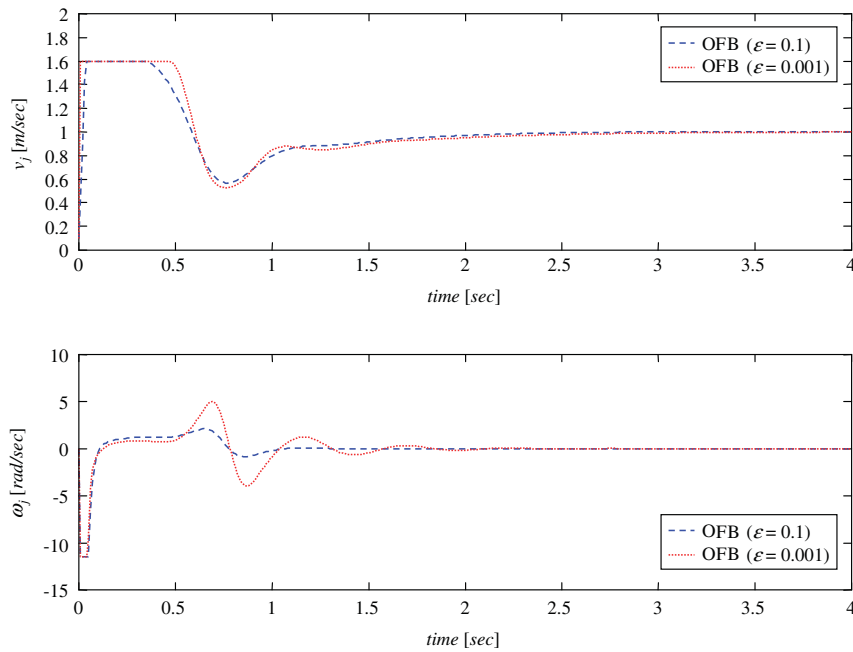


Figure 6. Control effort comparison with $\epsilon = 0.1, 0.001$ for the straight line path case.

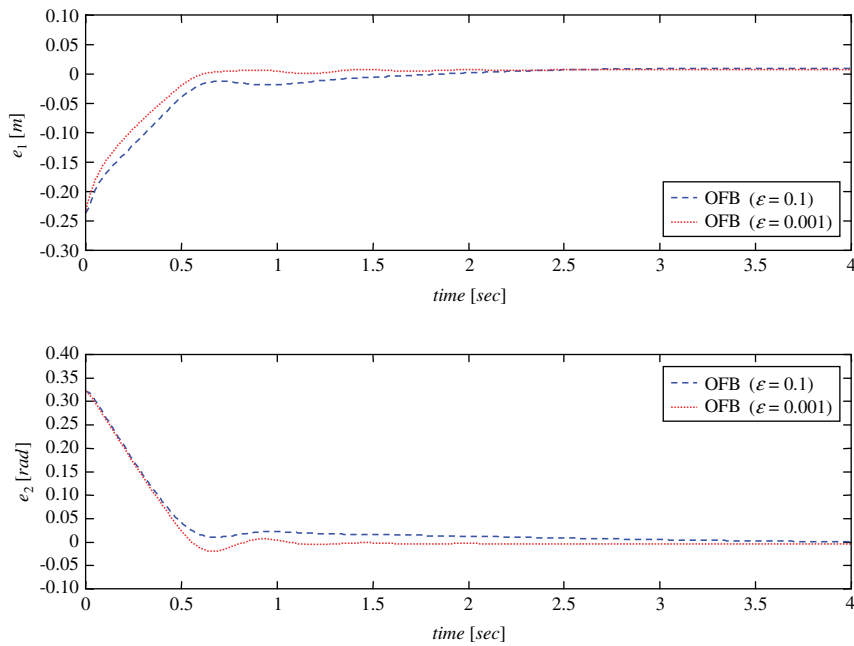


Figure 7. Output error comparison with $\epsilon = 0.1, 0.001$ for the straight line path case.

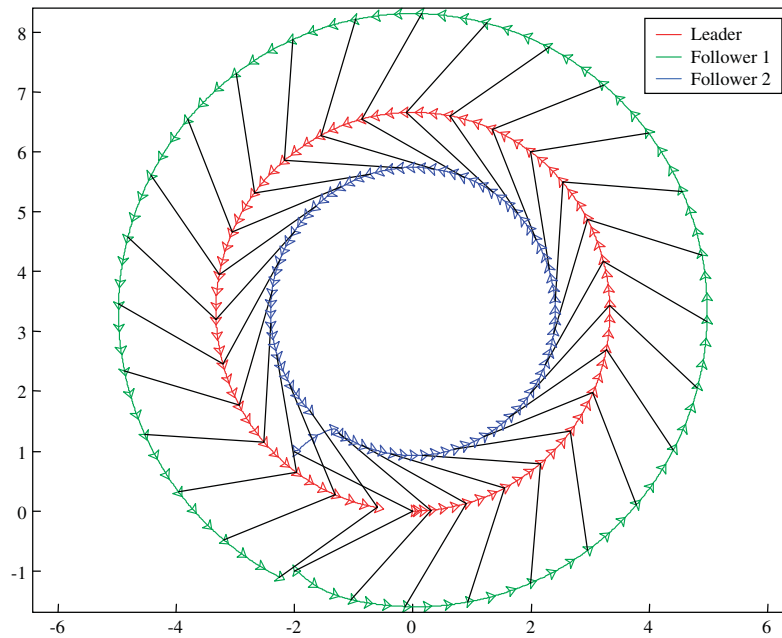


Figure 8. Trajectories of the leader robot and two followers for the circular path case.

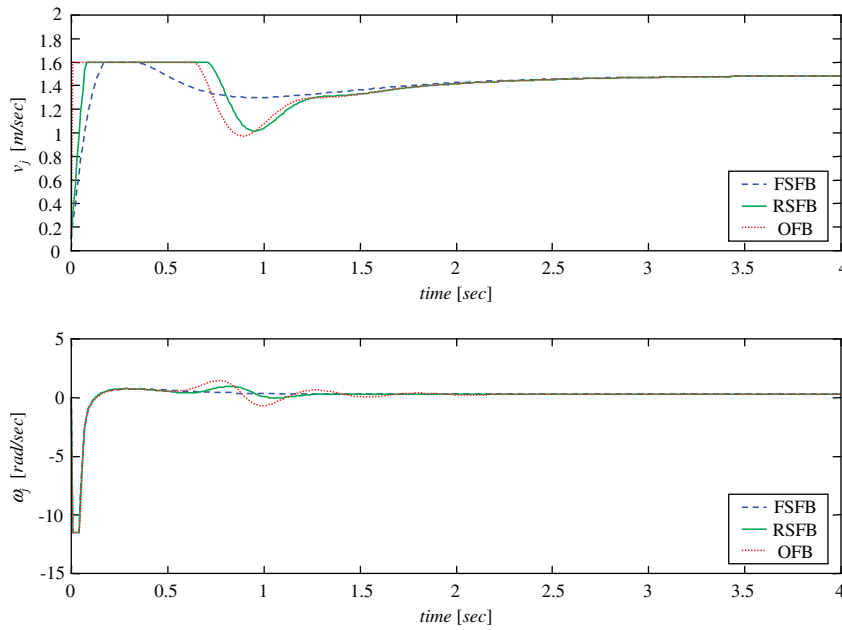


Figure 9. Velocity comparison between controllers (20), (22), and (42) for the circular path case.

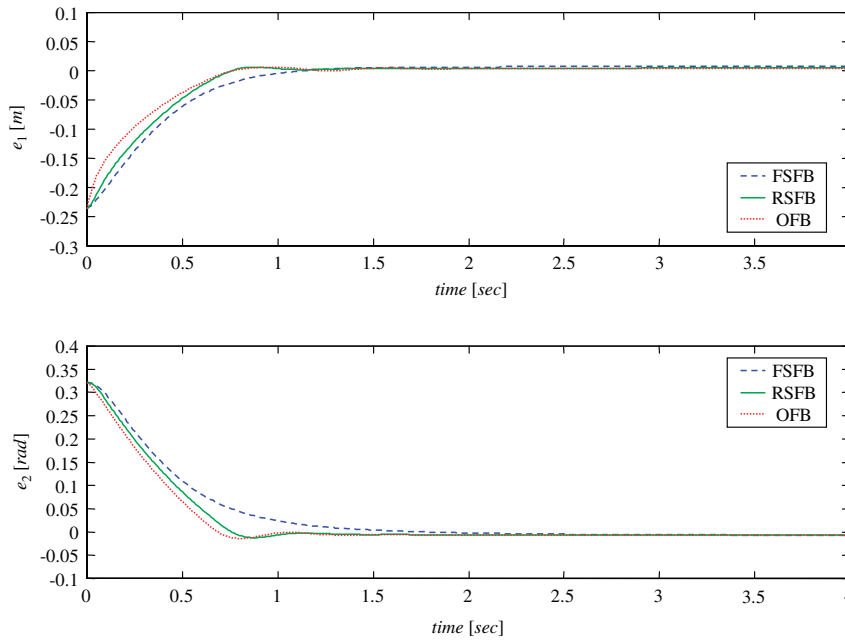


Figure 10. Output error comparison between controllers (20), (22), and (42) for the circular path case.

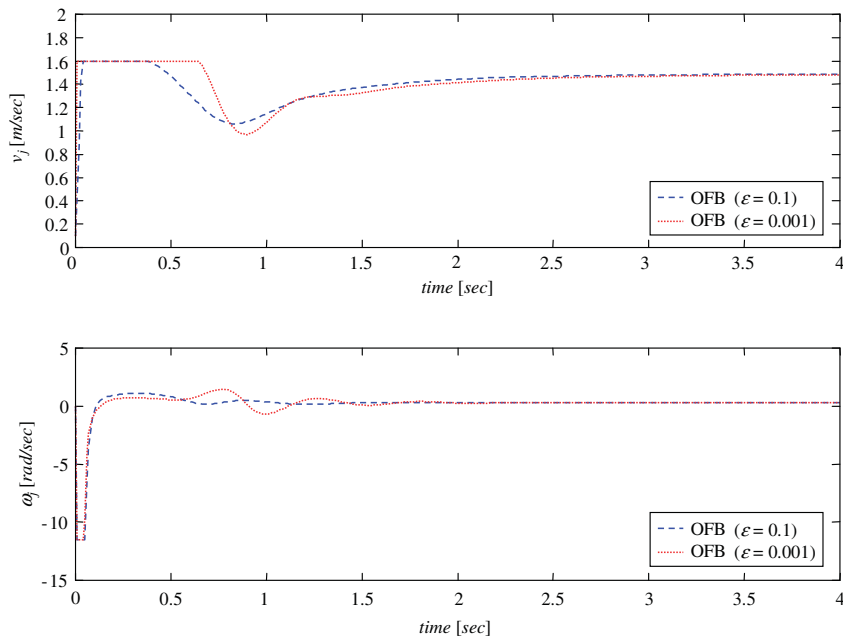


Figure 11. Control effort comparison with $\epsilon = 0.1, 0.001$ for the circular path case.

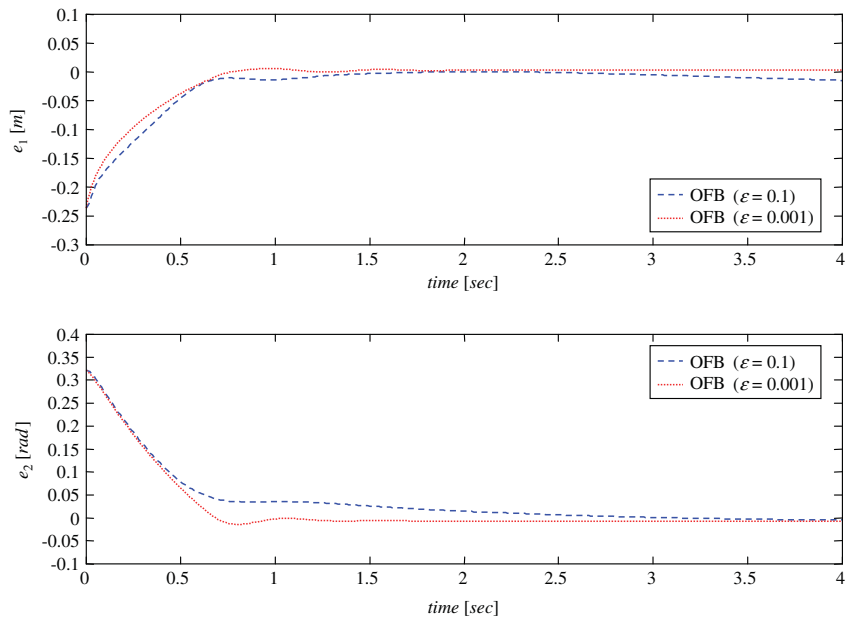


Figure 12. Output error comparison with $\epsilon = 0.1, 0.001$ for the circular path case.

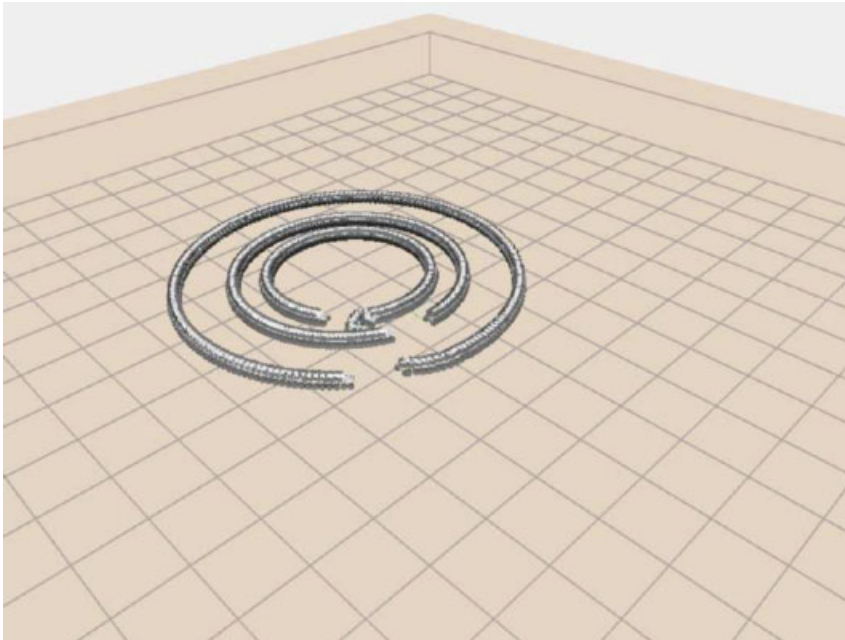


Figure 13. Snake view of the simulation with three robots.

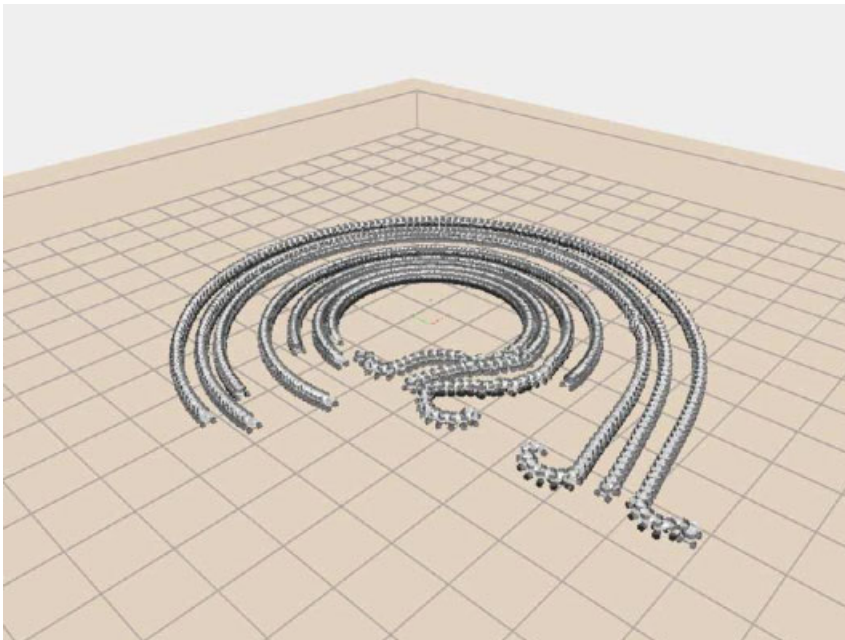


Figure 14. Snake view of the simulation with seven robots.

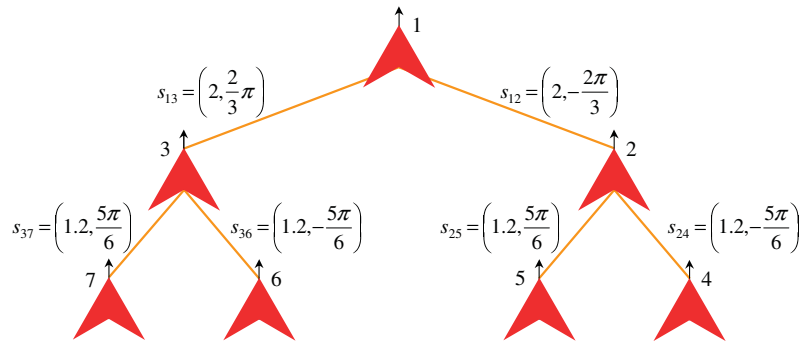


Figure 15. Edge specification for the simulation with seven robots.

Simulations in a realistic 3D environment verified the performance of all the formation controllers. Currently, the multi-vehicle decentralized control methodology is being tested on actual car-like mobile robots. Future research will focus on the analysis of input-to-state stability properties of this controller [18], effects of formation reconfiguration on the connectivity and stability of the communication graph and control graph, respectively.

APPENDIX A

A.1. Proof of Lemma 4.1

Let $P_L(t)$ be defined by

$$P_L(t) := \int_{t_0}^t L(\tau) d\tau$$

Substituting (18) into (25) and integrating in time,

$$\begin{aligned}
 P_L(t) &= \int_{t_0}^t \frac{de^T(\tau)}{d\tau} g_v(\tau) V_i(\tau) d\tau - \beta \int_{t_0}^t \frac{de^T(\tau)}{d\tau} \text{sign}(e(\tau)) d\tau \\
 &\quad + \int_{t_0}^t e^T(\tau) K^T g_v(\tau) V_i(\tau) d\tau - \beta \int_{t_0}^t e^T(\tau) K^T \text{sign}(e(\tau)) d\tau \tag{A1}
 \end{aligned}$$

with $g_v(t) = g_v(z_{ij}(t), v_j(t))$. Integrating by parts the first term on the right-hand side of (54)

$$\begin{aligned}
 P_L(t) &= e^T(t) g_v(t) V_i(t) - e^T(t_0) g_v(t_0) V_i(t_0) \\
 &\quad - \int_{t_0}^t e^T(\tau) \frac{d[g_v(\tau) V_i(\tau)]}{d\tau} d\tau - \beta \int_{t_0}^t \frac{de^T(\tau)}{d\tau} \text{sign}(e(\tau)) d\tau \\
 &\quad + \int_{t_0}^t e^T(\tau) K^T g_v(\tau) V_i(\tau) d\tau - \beta \int_{t_0}^t e^T(\tau) K^T \text{sign}(e(\tau)) d\tau
 \end{aligned}$$

Since $K = K^T$ and $\int_{t_0}^t (de^T(\tau)/d\tau) \text{sign}(e(\tau)) d\tau = \|e(t)\|_1 - \|e(t_0)\|_1$, we have

$$\begin{aligned} P_L(t) &= \beta \|e(t_0)\|_1 - e^T(t_0)g_v(t_0)V_i(t_0) + e^T(t)g_v(t)V_i(t) - \beta \|e(t)\|_1 \\ &\quad + \int_{t_0}^t e^T(\tau)K \left\{ g_v(\tau)V_i(\tau) - \beta \text{sign}(e(\tau)) - K^{-1} \frac{d}{d\tau} [g_v(\tau)V_i(\tau)] \right\} d\tau \\ &= \zeta_b + e^T(t)g_v(t)V_i(t) - \beta \|e(t)\|_1 \\ &\quad + \int_{t_0}^t e^T(\tau)K \left\{ g_v(\tau)V_i(\tau) - \beta \text{sign}(e(\tau)) - K^{-1} \frac{d}{d\tau} [g_v(\tau)V_i(\tau)] \right\} d\tau \end{aligned}$$

with $\zeta_b \triangleq \beta \|e(t_0)\|_1 - e^T(t_0)g_v(t_0)V_i(t_0)$.

As it can be seen, if β is chosen such that

$$\beta > \|g_v(t)V_i(t)\|_2 + k_{12}^{-1} \left| \frac{d[g_v(t)V_i(\tau)]}{dt} \right|_2$$

with $k_{12} := \min(k_1, k_2)$, then the second and third right-hand terms are less than zero. Hence,

$$\int_{t_0}^t L(\tau) d\tau < \zeta_b$$

ACKNOWLEDGEMENTS

This work is supported in part by NSF grants #0311460 and CAREER #0348637 and by the U.S. Army Research Office under grant DAAD19-03-1-0142 (through the University of Oklahoma).

REFERENCES

1. Fierro R, Chaimowicz L, Kumar V. Multi-robot cooperation. In *Autonomous Mobile Robots: Sensing, Control, Decision Making and Application*, Ge S, Lewis F (eds), Chapter 11. CRC Press: Boca Raton, FL, Taylor & Francis: London, 2006; 417–459.
2. Bullingham J, Richards A, How J. Receding horizon control of autonomous aerial vehicles. *Proceedings of the American Control Conference*, Anchorage, AK, May 2002; 3741–3746.
3. Ousingsawat J, Campbell M. Establishing optimal trajectories for multi-vehicle reconnaissance. *Proceedings of the AIAA Guidance, Navigation and Control Conference*, Providence, RI, August 2004 (CD-ROM).
4. Zelinski S, Koo T, Sastry S. Optimization-based formation reconfiguration planning for autonomous vehicles. *Proceedings of the IEEE International Conference on Robotics and Automation*, Taipei, Taiwan, September 2003; 3758–3763.
5. Das A, Fierro R, Kumar V, Ostrowski J, Spletzer J, Taylor C. A vision-based formation control framework. *IEEE Transactions on Robotics and Automation* 2002; **18**(5):813–825.
6. Das A. A framework for control of formations of mobile robots: theory and experiments. *Ph.D. Thesis*, Mechanical Engineering and Applied Mechanics, University of Pennsylvania, Pennsylvania, 2003.
7. Jadbabaie A, Lin J, Morse A. Coordination of groups of mobile autonomous agents using nearest neighbor rules. *IEEE Transactions on Automatic Control* 2003; **48**:988–1001.
8. Lawton J, Young B, Beard R. A decentralized approach to formation maneuvers. *IEEE Transactions on Automatic Control* 2003; **19**:933–941.
9. Moshtagh N, Jadbabaie A, Daniilidis K. Vision-based distributed coordination and flocking of multi-agent systems. *Proceedings of the Robotics: Science and Systems*, Cambridge, U.S.A., June 2005; 41–48.
10. Chen X, Serrani A, Özbay H. Control of leader–follower formations of terrestrial UAVs. *Proceedings of the 42nd IEEE Conference on Decision and Control*, vol. 1, Maui, Hawaii, U.S.A., December 2003; 498–503.

11. Vidal R, Shakernia O, Sastry S. Formation control of nonholonomic mobile robots with omnidirectional visual servoing and motion segmentation. *Proceedings of the IEEE International Conference on Robotics and Automation*, vol. 1, Taipei, Taiwan, September 2003; 584–589.
12. Cowan N, Shakerina O, Vidal R, Sastry S. Vision-based follow-the-leader. *Proceedings of the 2003 IEEE/RSJ International Conference on Intelligent Robots and Systems (IROS 2003)*, vol. 2, Las Vegas, NA, U.S.A., October 2003; 1796–1801.
13. Tang C-P, Bhatt R, Krovi V. Decentralized kinematic control of payload by a system of mobile manipulators. *Proceedings of the 2004 IEEE International Conference on Robotics and Automation*, vol. 3, New Orleans, LA, U.S.A., 2004; 2462–2467.
14. Gerkey B, Matarić M. Pusher-watcher: an approach to fault-tolerant tightly-coupled robot coordination. *Proceedings of the IEEE International Conference on Robotics and Automation*, vol. 1, Washington, DC, 2002; 464–469.
15. Young B, Beard R, Kelsey J. A control scheme for improving multi-vehicle formation maneuvers. *Proceedings of the American Control Conference*, vol. 2, Arlington, VA, U.S.A., June 2001; 704–709.
16. Diestel R. *Graph Theory* (3rd edn). Graduate Texts in Mathematics, vol. 173, Springer: Heidelberg, 2005.
17. Tanner H, Pappas G, Kumar V. Leader-to-formation stability. *IEEE Transactions on Robotics and Automation* 2004; **20**:443–455.
18. Tanner H. ISS properties of nonholonomic vehicles. *Systems and Control Letters* 2004; **53**:229–235.
19. David P, DeMenthon D, Duraiswami R, Samet H. SoftPOSIT: simultaneous pose and correspondence determination. *International Journal of Computer Vision* 2004; **59**:259–284.
20. Slotine J, Li W. *Applied Nonlinear Control*. Prentice-Hall: Englewood Cliffs, NJ, 1991.
21. Desai J, Ostrowski J, Kumar V. Modeling and control of formations of nonholonomic mobile robots. *IEEE Transactions on Robotics and Automation* 2001; **17**:905–908.
22. Lewis F, Abdallah C, Dawson D. *Control of Robot Manipulators*. Macmillan: New York, 1993.
23. Khalil H. *Nonlinear Systems* (3rd edn). Prentice-Hall: Englewood Cliffs, NJ, 2002.
24. Orqueda O. Software and algorithms for motion planning in virtual environments. In *Computational Mechanics*, Rosales VHCMB, Bambill BDV (eds), vol. XXII, Argentina, 2003.
25. Orqueda O. Motion planning and control of autonomous robots. *Doctoral Thesis*, Department of Electrical and Computer Engineering, Universidad Nacional del Sur, Bahía Blanca, Argentina, August 2006 (in Spanish).